Deterministic indoor wave propagation modeling

LAJOS NAGY

Budapest University of Technology and Economics,
Department of Broadband Infocommunications and Electromagnetic Theory
lajos.nagy@mht.bme.hu

Keywords: indoor propagation, diffraction, FDTD, ray tracing

The next generation mobile access network system design needs more precise characterization of the radio channel and needs sophisticated propagation models, because of the decreasing cell sizes and of higher data rates. In particular, the planning of the coverage in tunnels and indoor spaces causes design problems without these models. Indoor propagation problems for wideband radio systems are widely investigated and one of the today applied approach of modeling is the ray-tracing, ray-launching method. These ray methods are efficient for parallel-perpendicular scenarios but there is a common problem when tracing the rays for curved surfaces. The other disadvantage of the ray methods is the difficulty in describing the diffraction for a complex scenario. The specific case of the straight circular tunnel can be modeled analytically as a waveguide with circular cross-section. Each of the two previous models has a disadvantage by modeling our problem: the ray tracing needs huge running time because on the curved surface reflection the number of rays in bundles has to be increased, whilst the analytical method is not able to handle the complex propagation problem in presence the vehicle. In our investigation the Finite Difference Time Domain method was proposed and used to analyze the 2 and 3 dimensional indoor wave propagation problems. We demonstrate the efficiency and flexibility of FDTD for curved tunnel, indoor office and special EMC cases [11-13].

1. Introduction

In the radio network design practice empirical, semi-empirical and deterministic radio wave propagation methods are used for field strength estimation. The designers of the 3rd and 4th generation systems need broadband characterization of the radio channel and coverage prediction, which is based on any deterministic propagation model. The receiver designers also need precise stochastic description of the radio channel to develop the equalizer and estimation of the receiver.

The indoor base station and radio access points are usually used to extend coverage to indoor areas where outdoor signals do not reach well, or to add network capacity in areas with very dense mobile device usage. These cells in the mobile structure are called as pico-cells. In the dense subscriber environments the precise coverage prediction has an increased importance, and the empirical and semi-empirical models are not able to guarantee the necessary accuracy.

The deterministic models generally based on ray tracing or on direct solution of the Maxwell's equations. The first step of the ray tracing methods is solving a pure geometrical problem, but in special cases this leads to very complex analysis especially for curved building geometries, highway and underground tunnels, and for highly reflective building media, like reinforced concrete. In such cases the tracing and storing of few million rays results in huge memory requirement and calculation time for multiple reflection, transmission and diffraction. The other disadvantage of the ray methods is the difficulty in describing the diffraction for a complex scenario. In related papers [1] ray tracing method introduced where bundles of rays are used to represent each "physical" wave. Monte Carlo techniques were used for the ray launching. Each bundle of rays was traced to a receiver position where reception spheres determined which rays are intercepted by the receiver.

The Maxwell's equations can be solved directly using parabolic type equations or in differential form using Finite Difference Time Domain (FDTD) method [5].

The main aim of this article is to introduce the FDTD method and to demonstrate its suitability in solving radio wave propagation problems. The application areas are individually introduced and demonstrated by examples, of which the memory and simulation time requirements are also analyzed. First the radio wave propagation physical mechanisms are summarized, which are also used by the ray tracing method for modeling wave material interaction. The next section summarizes the most important empirical and deterministic indoor propagation models, and the FDTD will be introduced briefly for general three-dimensional case in rectangular coordinate system and for two special two dimensional geometries. Section 4 discusses the data base requirements of building geometries for indoor radio wave propagation modeling, and the last part of the paper introduces the simulation results.

2. Wave propagation mechanisms

The effect of difficult and complex geometry of radio wave propagation environment can be simplified to simple physical models as direct, reflected, transmitted and diffracted paths. The ray tracing propagation mo-

deling method means solving the geometrical problem first, and after partitioning the wave into rays the simple physical methods above are used to describe the interaction between the propagating waves and materials.

2.1. Direct path

The direct path means considering the propagation in Line of Sight (LOS), where the receiver is in direct visibility with the transmitter. In terms of radio wave propagation, being in LOS means having the Fresnel zones cleared all along the path.

If the transmitter antenna of gain G_A is fed by P_A input power, then the radiated power density at a distance r assuming LOS spherical wave propagation would be

$$S_o = \frac{P_A G_A}{4\pi r^2} \tag{1}$$

In the far field region of the transmitter antenna the electric and magnetic field strength vectors are mutually perpendicular to each other and of propagation direction, and are in phase. Therefore the power density can be described as

$$S_o = \frac{|\mathbf{E}|^2}{240\pi} \tag{2}$$

The electrical field strength magnitude can be derived from (1) and (2) as

$$E = \frac{\sqrt{60 P_A G_A}}{r} \tag{3}$$

Expression (3) shows that the electrical field strength magnitude is inversely proportional to the distance, for spherical waves, and the received power is inversely proportional to the square of the distance. For the two-dimensional problem, the electrical field strength dependence is $E \approx 1/\sqrt{r}$ in case of cylindrical wave.

2.2. Reflection

Reflection occurs when a propagating electromagnetic wave impinges upon an object which has very large dimensions when compared to the wavelength of the propagating wave. Reflections occur from the surface of the earth and from buildings and walls. The amplitude, phase and polarization of the reflected wave depend on material parameters of the reflecting medium and on the surface irregularity. If the interaction surface is plane and perfectly smooth then the specular reflection is observed and the energy flow is discrete in space. This ideal case can be modeled using the Snell-Descartes law extended for lossy dielectrics. In most cases of the radio wave propagation problems the medium is diamagnetic or nonmagnetic so its relative permeability is 1.

The reflection coefficient for plane waves is defined as the complex electric field strength ratio of the incoming and the reflected wave ($R = E_r / E_i$), which is decomposed into its perpendicular and parallel components *(Figure 1)*. The reflection coefficients for the two polarization states are:

$$R_\perp = \frac{\cos\vartheta - \sqrt{\varepsilon_r + \cos^2\vartheta - 1}}{\cos\vartheta + \sqrt{\varepsilon_r + \cos^2\vartheta - 1}}$$
$$R_\parallel = \frac{\varepsilon_r \cos\vartheta - \sqrt{\varepsilon_r + \cos^2\vartheta - 1}}{\varepsilon_r \cos\vartheta + \sqrt{\varepsilon_r + \cos^2\vartheta - 1}} \tag{4}$$

where ε_r is the ratio of the complex dielectric material parameters for the two media on the planar interface.

Figure 2 shows the stationary field excited by a $\perp$ polarized point source in the upper half plane, with sinusoidal time dependence.

The reflection material's complex permittivity is ε_r = 3-1*j, and the area of investigation is 10λ*15λ. The typical interference picture shows wave front undulation and significant field strength decreasing in several directions.

Figure 2. Direct and reflected field component interference

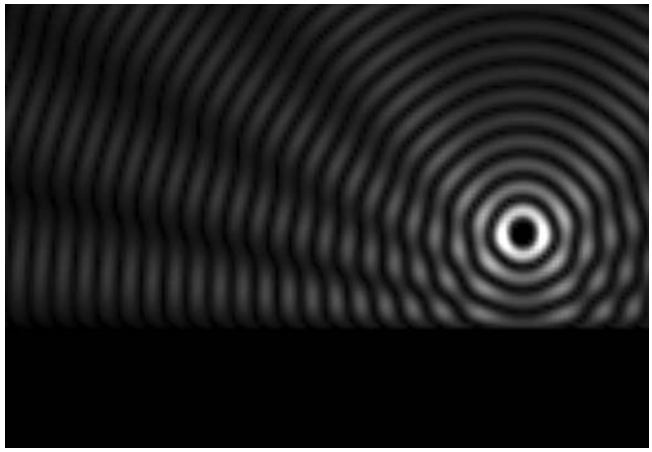

Figure 1. Perpendicular $\perp$ (hard) and parallel $\parallel$ (soft) polarization

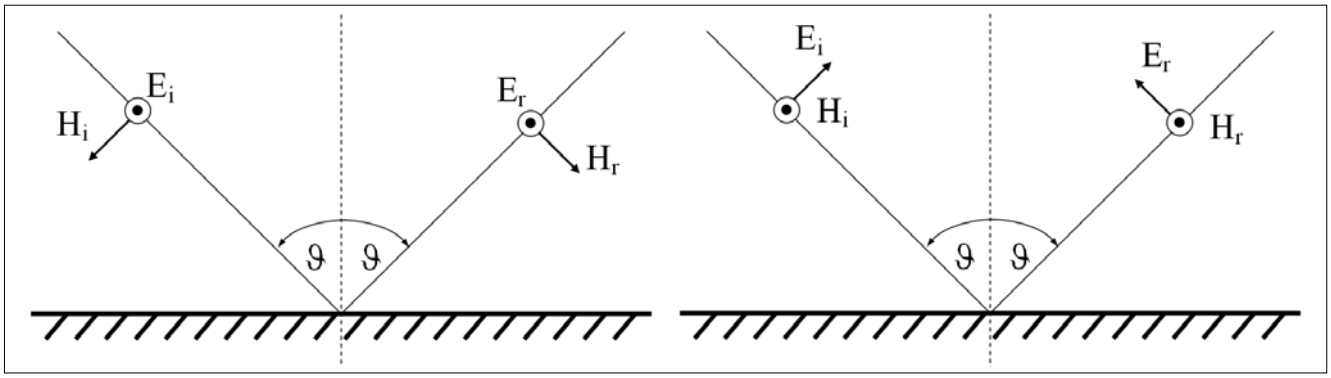

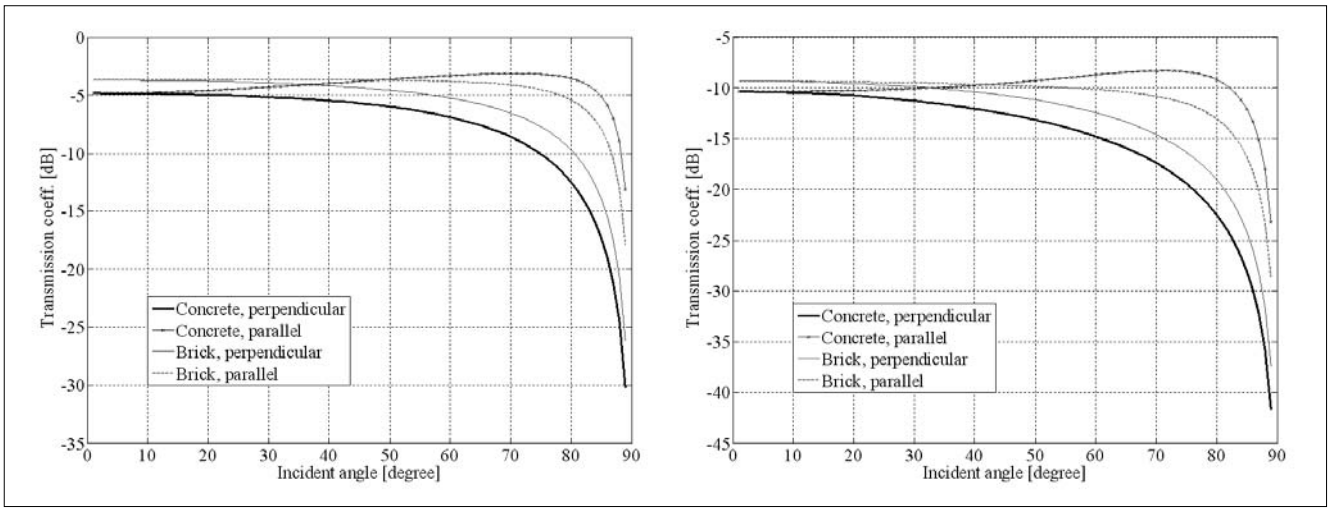

Figure 3. Transmission coefficients at 900 MHz and 2.4 GHz

2.3. Transmission

The transmission coefficient (throughput loss), $T = E_t / E_i$, is used to represent the electrical field strength ratio of the electromagnetic incident and transmitted wave at the interface of two media.

General formulation of the reflection and transmission coefficients of multiple material layers can be developed for uniform plane wave at oblique angle incidence using the transmission line theory. The model is based on the well known impedance transfer equation for transmission lines with different characteristic impedance [9]. The results in *Figure 3* present the simulated transmission coefficients as a function of the wave incidence angle for brick and concrete slabs bounded on both sides of air. The concrete and brick slab thicknesses are 12 cm with complex permittivity of ε_r = 9 -i *0.9 and ε_r = 2.8 -i*0.56 respectively.

The results show no significant difference in transmission coefficients for brick and concrete but this loss highly increases with frequency, therefore especially WLAN network areas are limited by this factor in multiple wall indoor environment. (The reinforced concrete iron layer produces additional reflection and transmission loss which can be modeled using FDTD simulation.)

The ray tracing method also uses the multiple layer transmission calculation but this simplification results in increasing error for short range radio environments where the material interfaces are in near field of the antennas or there are not bounded by plane surfaces.

The FDTD method is able to model also the previous cases, as well as the case of excitation by non sinusoidal time dependent source. *Figure 4* shows the field strength distribution for Gaussian pulse modulated sinusoidal excitation at different time with interaction of the wave by finite thickness lossy dielectric slab having permittivity of ε_r = 3-1*j. The wave decoupling into reflected and transmitted components is obvious.

2.4. Diffraction

Diffraction refers to the bending of waves around an edge of an object. Diffraction phenomenon depends on the size of the object relative to the wavelength of

Figure 5/a. Direct, reflection and diffraction regions

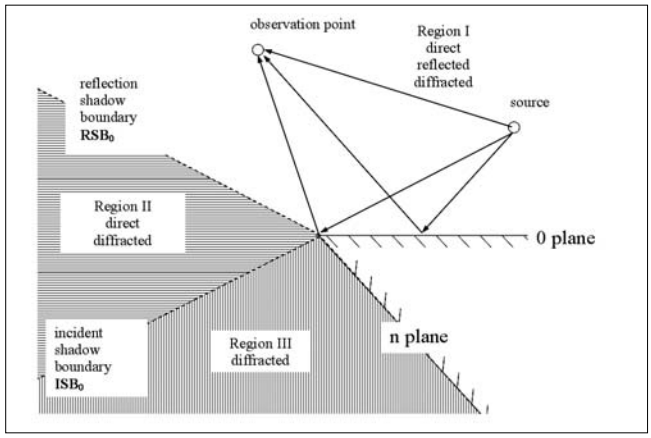

Figure 4. Wave transmission on finite thickness lossy dielectric excited by point source with ⊥ polarization

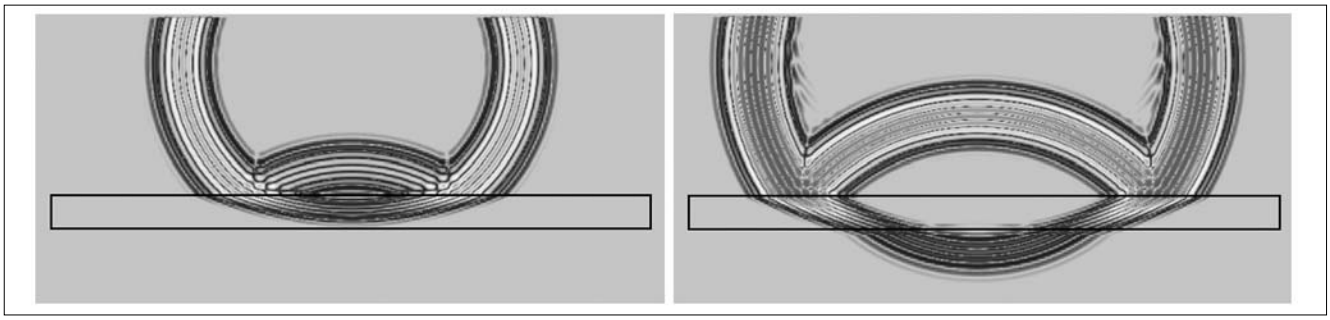

the wave. When the dimensions of the radiating object are large compared to the wavelength, high frequency asymptotic techniques can be used to analyze many, otherwise mathematically not treatable problems. Basically the application of the diffraction theory was started in the area of physics which deals with the description of the light wave propagation.

The basic concept of geometrical optics, or ray optics is in many situations inadequate to completely describe the behavior of the electromagnetic field in the shadow region, behind the diffraction objects. The diffracted field is added to calculate the field contribution in the shadow region, and that permits us to solve many practical radio wave propagation problems.

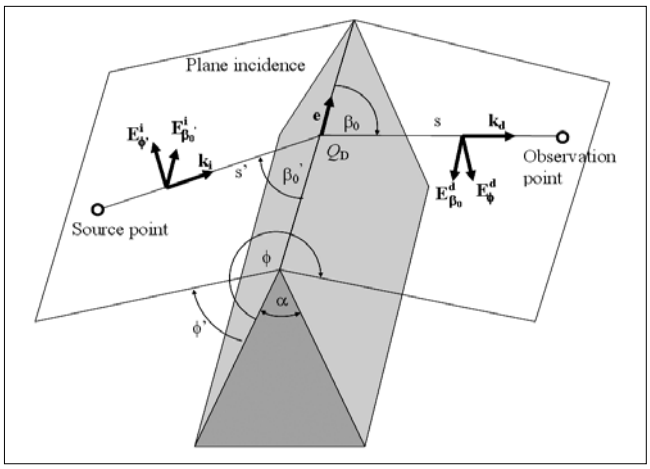

Figure 5/b. Diffraction geometry

The diffraction components are expressed as

$$\begin{bmatrix} \mathbf{E}^d_{\beta_0}(s) \\ \mathbf{E}^d_{\phi}(s) \end{bmatrix} = -\begin{bmatrix} D_s & 0 \\ 0 & D_h \end{bmatrix} \begin{bmatrix} \mathbf{E}^i_{\beta_0'}(Q_D) \\ \mathbf{E}^i_{\phi'}(Q_D) \end{bmatrix} A(s',s)e^{-jks} \tag{5}$$

where

$\mathbf{E}^i_{\beta_0'}(Q_D)$ the component of incident electrical field parallel to the plane of incidence at the point of diffraction,

$\mathbf{E}^i_{\phi'}(Q_D)$ the component of incident electrical field perpendicular to the plane of incidence at the point of diffraction, D_s and D_h are the diffraction coefficients for soft and hard polarization.

$$A(s',s) = \begin{cases} \dfrac{1}{\sqrt{s \cdot \sin\beta_0}} & \text{for cylindrical incoming waves} \\ \sqrt{\dfrac{s'}{s(s+s')}} & \text{for spherical incoming waves} \end{cases}$$

The expression of diffraction coefficients are first derived by Keller [9] publishing the Geometrical Theory of Diffraction (GTD). The GTD diffraction coefficients possess singularities along the incident and reflection shadow boundaries and therefore in the neighborhood of these boundaries the model is inapplicable.

In the later work of Kouyoumjian and Pathak, the singularities were removed by introducing the Uniform Theory of Diffraction (UTD) and this approach is used in most wave propagation models. The regions in the neighborhood of the shadow boundaries are referred to as transition regions, and in these regions the fields undergo their most rapid changes. The diffraction coefficients are

$$D_h(\phi,\phi',n,\beta'_0) = \frac{e^{-j\pi/4}}{2n\sqrt{2\pi k}\sin\beta'_0}\left[D_0^{ISB} + D_n^{ISB} + R_0^h D_0^{RSB} + R_n^h D_n^{RSB}\right]$$

$$D_s(\phi,\phi',n,\beta'_0) = \frac{e^{-j\pi/4}}{2n\sqrt{2\pi k}\sin\beta'_0}\left[D_0^{ISB} + D_n^{ISB} + R_0^s D_0^{RSB} + R_n^s D_n^{RSB}\right] \tag{6}$$

where $R_0^{h,s}$ and $R_n^{h,s}$ are the reflection coefficients on 0 and *n* planes represented in *Figure 5/a*, $D_{0,n}^{ISB,RSB}$ are the incident diffraction coefficient component at the Incident Shadow Boundary (ISB) and the reflected diffracted component at the Reflection Shadow Boundary (RSB), respectively.

Figure 6 shows a propagating wave before and after the diffraction on a lossy dielectric wedge for Gaussian modulated sinusoidal point source excitation and simulated by FDTD method.

2.5. Scattering

Rough surfaces and finite surfaces scatter the incident energy in all directions with a radiation diagram which depends on the roughness and size of the surface or volume. The dispersion of energy through scat-

Figure 6. Diffraction on a lossy dielectric wedge

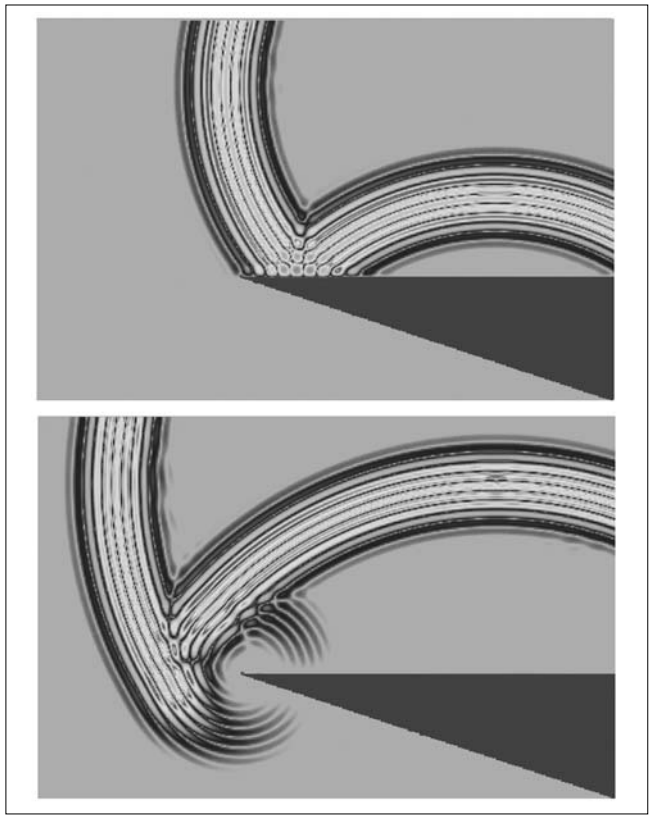

tering means a decrease of the energy reflected in the specular direction. This simple view leads to account for the scattering process only by decreasing the reflection coefficient and thus, only by multiplying the reflection coefficient with a factor smaller than one, which, according to the Raleigh theory, depends exponentially on the standard deviation of the surface roughness.

3. Wave propagation models

To implement a mobile radio system, wave propagation models are necessary to determine propagation characteristics for signal and interference powers and for any arbitrary installation and any receiving positions. These models and results are the basis for the high-level network planning process. The narrow-band signals and simple building geometry make possible to apply empirical and semi-empirical models in the network design practice. The need for using deterministic models is mainly caused by the building complexity, and by the broadband or time dependent characterization of the radio channel.

3.1. Empirical and semi-empirical models

The various empirical and semi-empirical indoor propagation models use two approaches. The first is to model the propagation loss by a path loss law model determining the propagation exponent from measurements. The second one is a more successful approach to characterize indoor path loss by a fixed path loss exponent, plus additional loss factors related to the number of floors and walls intersected by the straight line between the access point and terminals. The two widely used models belonging to the second approach are the Motley-Keenan and the COST231 [10] models.

The path loss expression from the Motley-Keenan model for path distance r is:

$$L^{dB} = L_1 + 20\log r + n_f a_f + n_w a_w \tag{7}$$

where

L_1 is the loss at $r = 1$ m,
a_f and a_w are the attenuation factors (in dB) per floor and per wall respectively,
n_f and n_w are the number of floors and walls intersected by the radio path.

The path loss of the COST231 multi-wall model is:

$$L = L_F + L_c + \sum_{i=1}^{W} L_{wi} n_{wi} + L_f n_f^{\left[\frac{(n_f+2)}{(n_f+1)}-b\right]} \tag{8}$$

where

L_F is the free space path loss for the straight line path,
L_c and b are empirically derived constants.

Table 1. Recommended parameters of the COST231 multi-wall indoor model for 1800 MHz

L_w	L_f	B
Light wall 3.4 dB Heavy walls 6.9 dB	18.3 dB	0.46

3.2. Deterministic models

Ray tracing

The ray tracing type radio wave propagation models are based on geometrical optics, instead of the entire domain field simulation. The method partitions the propagation waves into finite angular components, and these propagation components are traced independently and are applied to each the boundary conditions on material interfaces – reflection, transmission, diffraction. The solution on every observation points can be finally derived by summing the wave contributions.

Figure 7.
First and second order ray tracing components

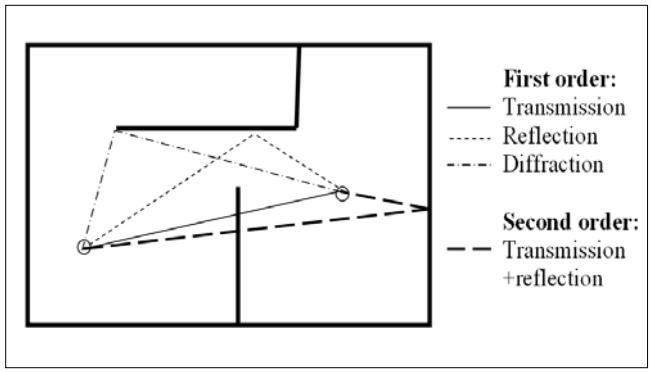

The ray tracing method in practice uses either all possible first, second and third order combination of propagation mechanisms, or the ray components are traced till the field strength reaches a user defined threshold limit.

FDTD method

The FDTD (Finite Difference Time Domain) method is a time domain solution of the Maxwell's equations described in differential form and is widely used in circuit analysis because of its simplicity. The method divides the space investigated into finite grid elements and on the grid the time and space approximation of the electrical and magnetic field strength is performed [5].

There exist many various forms of the FDTD in one, two or three dimensions and for many coordinate systems or grids and material types. For the indoor wireless channel simulation the three dimensional rectangular coordinate system was chosen with linear lossy dielectric materials in volumes.

Table 2. Ray tracing and FDTD method comparison

	Ray tracing	FDTD
Features	Frequency domain solution; Narrowband, harmonic excitation	Time domain solution; Broadband, arbitrary excitation
Advantages	The problem can be split into parts	Simple programming; Simple data base structure with volume elements;
Disadvantages	Difficulty in programming; In case of complex or rounded geometry the significant divergence of traced rays; Data base pre processing needed – the volume element have to be dissolve into boundary surface elements; Tremendous running time;	Tremendous running time and memory requirement

The method will be introduced briefly for the general three-dimensional case in rectangular coordinate system.

Starting from the generalized differential matrix operators, the Maxwell's curl equations can be expressed in the rectangular coordinate system as

$$\frac{\partial E_x}{\partial t} = \frac{1}{\varepsilon}\left[\frac{\partial H_z}{\partial y} - \frac{\partial H_y}{\partial z} - \left(J_{source_x} + \sigma E_x\right)\right]$$

$$\frac{\partial E_y}{\partial t} = \frac{1}{\varepsilon}\left[\frac{\partial H_x}{\partial z} - \frac{\partial H_z}{\partial x} - \left(J_{source_y} + \sigma E_y\right)\right] \qquad (9)$$

$$\frac{\partial E_z}{\partial t} = \frac{1}{\varepsilon}\left[\frac{\partial H_y}{\partial x} - \frac{\partial H_x}{\partial y} - \left(J_{source_z} + \sigma E_z\right)\right]$$

Then the Yee algorithm [5] is used for a discrete grid and, considering a substitution of central differences for the time (∂/∂t) and space (∂/∂x, ∂/∂y, ∂/∂z) derivatives in (9), one gets for the time marching solution of the following coupled equations. The algorithm defines the six (E_x, E_y, E_z, H_x, H_y, H_z) discretized field components in the FDTD rectangular unit cell (the Yee cell). This cell has dimensions of $\Delta x\Delta y\Delta z$ and the electric and magnetic field components locations are interleaved by half of the discretization length ($\Delta x/2$,$\Delta y/2$ and Δz).

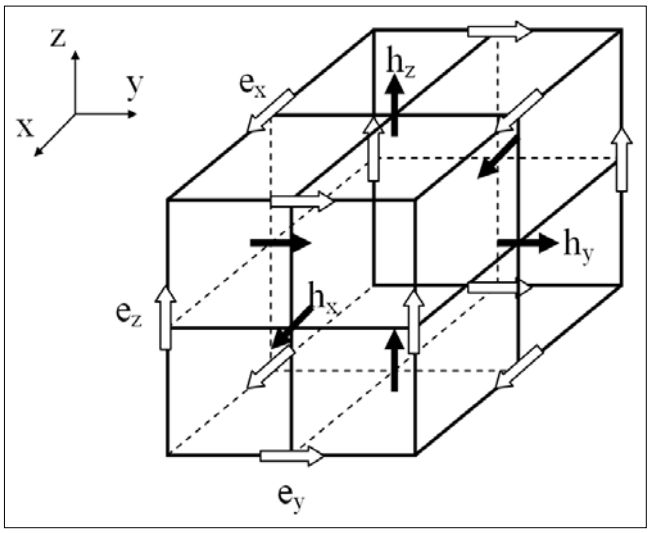

Figure 8. The 3 dimensional FDTD Yee cell with the electrical and magnetic reference vectors

In a similar manner calculating the fields every half-time step the centered difference for the time derivative is obtained.

The x directional electrical field strength component at the n+1/2 time step is:

$$E_x\big|_{i,j+1/2,k+1/2}^{n+1/2} = \left(\frac{1-\frac{\sigma_{i,j+1/2,k+1/2}\Delta t}{2\varepsilon_{i,j+1/2,k+1/2}}}{1+\frac{\sigma_{i,j+1/2,k+1/2}\Delta t}{2\varepsilon_{i,j+1/2,k+1/2}}}\right) E_x\big|_{i,j+1/2,k+1/2}^{n-1/2} + \left(\frac{\frac{\Delta t}{\varepsilon_{i,j+1/2,k+1/2}}}{1+\frac{\sigma_{i,j+1/2,k+1/2}\Delta t}{2\varepsilon_{i,j+1/2,k+1/2}}}\right) \cdot \left(\begin{array}{l} \frac{H_z\big|_{i,j+1,k+1/2}^{n} - H_z\big|_{i,j,k+1/2}^{n}}{\Delta y} \\ -\frac{H_y\big|_{i,j+1/2,k+1}^{n} - H_y\big|_{i,j+1/2,k}^{n}}{\Delta z} \\ - J_{source_x}\big|_{i,j+1/2,k+1/2}^{n} \end{array}\right) \qquad (10)$$

Similar finite difference equations can be expressed for the other five field strength components, E_y, E_z, H_x, H_y and H_z.

The discretization on the simulation volume is made by cubic lattice so $\Delta x = \Delta y = \Delta z = \Delta$ which results in a significant simplification of the finite difference equations.

The $\varepsilon_{i,j,k}$ and $\sigma_{i,j,k}$ are the permittivity and conductivity of the material at the i,j,k discretisation position.

Stability of the FDTD solution requires that the electromagnetic wave does not pass through more than one cell in one time step, i.e., the time step and the unit cell dimension satisfy the Courant condition.

The Δt time step was chosen in accordance of this magic time step

$$\Delta t \le \frac{1}{c\sqrt{\frac{1}{(\Delta x)^2}+\frac{1}{(\Delta y)^2}+\frac{1}{(\Delta z)^2}}} \qquad (11)$$

which results $\Delta t \le \Delta/(c\sqrt{3})$ for our cubic lattice.

Special two dimensional geometries

The first investigation showed that the determination of field strength distribution in tunnel using full 3D model extends our calculation possibilities. Therefore we decided to model our geometry in two cut planes, namely in the axial and in the radial plane. The two approximations differ basically because the axial cut plane can be applied in case of rotationally symmetric geometry and the radial plane is a cut of the tunnel waveguide which is assumed non changing cross section *(Figure 9)*.

Figure 9. Axial and radial cut planes

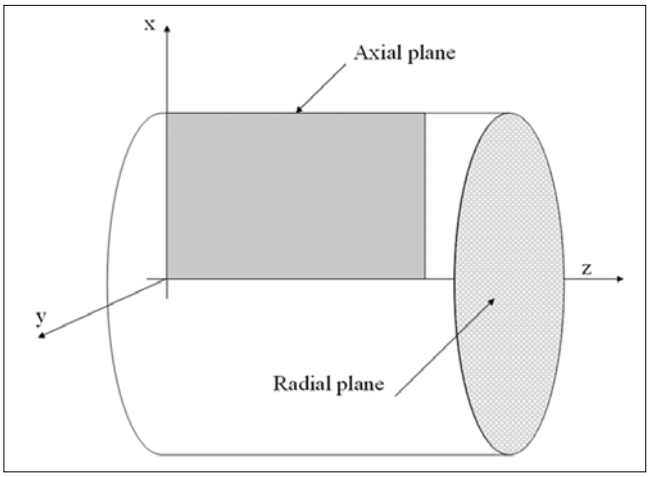

Axial plane

For the derivation of the cylindrical FDTD equations starting from the generalized differential matrix operators, we express the Maxwell's curl equations in the cylindrical coordinate system as

$$\nabla \times \mathbf{E} = \begin{vmatrix} \mathbf{e}_r & \mathbf{e}_\varphi & \frac{1}{r}\mathbf{e}_z \\ \frac{\partial}{\partial r} r & \frac{\partial}{\partial \varphi} & \frac{\partial}{\partial z} \\ E_r & E_\varphi & \frac{1}{r}E_z \end{vmatrix} = -\frac{\partial \mu \mathbf{H}}{\partial t} + \sigma^m \mathbf{H} \qquad (12)$$

$$\nabla \times \mathbf{H} = \begin{vmatrix} \mathbf{e}_r & \mathbf{e}_\varphi & \frac{1}{r}\mathbf{e}_z \\ \frac{\partial}{\partial r} r & \frac{\partial}{\partial \varphi} & \frac{\partial}{\partial z} \\ H_r & H_\varphi & \frac{1}{r}H_z \end{vmatrix} = \frac{\partial \varepsilon \mathbf{E}}{\partial t} + \sigma^e \mathbf{E} \qquad (13)$$

where

ε is the permittivity,

μ is the permeability,

σ^e is the electric conductivity,

σ^m is the magnetic conductivity.

The φ variation of **E** and **H** in the cylindrical coordinates system will have the following form

$$\mathbf{E},\mathbf{H} = \sum_{m=0}^{\infty} \left[(\mathbf{e}_u, \mathbf{h}_u) \cos m\varphi + (\mathbf{e}_v, \mathbf{h}_v) \sin m\varphi \right] \qquad (14)$$

where

m is the mode number.

Using the cylindrical symmetry of the geometry the 3D equations are reduced to 2D in the (x-z) r-z plane.

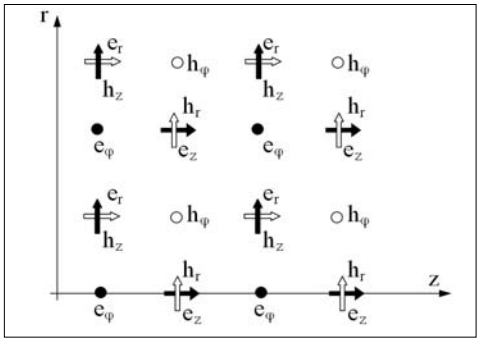

Figure 10. Electric and magnetic field components on the axial plane

After discretizing the equations 12-14 and applying the finite difference approximations to yield the updating equations for each field components [5]:

$$E_r\big|_{i,k}^{n+1} = \left(\frac{1-\frac{\sigma_r^e \Delta t}{2\varepsilon_0 \varepsilon_r}}{1+\frac{\sigma_r^e \Delta t}{2\varepsilon_0 \varepsilon_r}}\right) E_r\big|_{i,k}^{n} - \left(\frac{\frac{\Delta t}{\varepsilon_0 \varepsilon_r}}{1+\frac{\sigma_r^e \Delta t}{2\varepsilon_0 \varepsilon_r}}\right)\left[\frac{H_\varphi\big|_{i,k}^{n+1/2} - H_\varphi\big|_{i,k-1}^{n+1/2}}{\Delta z} - \frac{m}{(i)\Delta r} H_z\big|_{i,k}^{n+1/2}\right] \qquad (15)$$

$$E_\varphi\big|_{i,k}^{n+1} = \left(\frac{1-\frac{\sigma_\varphi^e \Delta t}{2\varepsilon_0 \varepsilon_\varphi}}{1+\frac{\sigma_\varphi^e \Delta t}{2\varepsilon_0 \varepsilon_\varphi}}\right) E_\varphi\big|_{i,k}^{n} + \left(\frac{\frac{\Delta t}{\varepsilon_0 \varepsilon_\varphi}}{1+\frac{\sigma_\varphi^e \Delta t}{2\varepsilon_0 \varepsilon_\varphi}}\right)\left(\frac{H_r\big|_{i,k}^{n+1/2} - H_r\big|_{i,k-1}^{n+1/2}}{\Delta z} - \frac{H_z\big|_{i,k}^{n+1/2} - H_z\big|_{i-1,k}^{n+1/2}}{\Delta r}\right) \qquad (16)$$

where

$$i = r/\Delta r\,,\quad k = z/\Delta z\,,\quad n = t/\Delta t$$

Radial plane

The main steps will be introduced briefly for the two-dimensional rectangular coordinate system. Starting from the generalized differential matrix operators, the Maxwell's equations can be express in the rectangular coordinate system as

For TM_z case:

$$\frac{\partial E_z}{\partial t} = \frac{1}{\varepsilon}\left[\frac{\partial H_y}{\partial x} - \frac{\partial H_x}{\partial y} - J_{source_z}\right]$$
$$-\mu \frac{\partial H_x}{\partial t} = \frac{\partial E_z}{\partial y} \qquad (17)$$
$$-\mu \frac{\partial H_y}{\partial t} = \frac{\partial E_z}{\partial x}$$

For TE_z case similar expressions can be introduced.

Then the Yee algorithm is used for a discrete grid and considering a substitution of central differences for the time and space derivatives in (17) one gets for the time marching solution of the following coupled equations [5]:

$$H_x\big|_{j+1/2,k}^{n+1/2} = H_x\big|_{j+1/2,k}^{n-1/2} - \frac{\Delta t}{\mu}\frac{E_z\big|_{j+1/2,k+1/2}^{n} - E_z\big|_{j+1/2,k-1/2}^{n}}{\Delta y} \qquad (18)$$

$$H_y\big|_{j,k+1/2}^{n+1/2} = H_y\big|_{j,k+1/2}^{n-1/2} + \frac{\Delta t}{\mu}\frac{E_z\big|_{j+1/2,k+1/2}^{n} - E_z\big|_{j-1/2,k+1/2}^{n}}{\Delta x} \qquad (19)$$

$$E_z\big|_{j+1/2,k+1/2}^{n+1} = \frac{1-\xi}{1+\xi} E_z\big|_{j+1/2,k+1/2}^{n} + \frac{1}{1+\xi}\frac{\Delta t}{\varepsilon}\frac{H_y\big|_{j+1/2,k+1}^{n+1/2} - H_y\big|_{j+1/2,k}^{n+1/2}}{\Delta x} - \frac{1}{1+\xi}\frac{\Delta t}{\varepsilon}\frac{H_x\big|_{j+1/2,k+1}^{n+1/2} - H_x\big|_{j+1/2,k}^{n+1/2}}{\Delta y} \qquad (20)$$

where

$$\xi = \frac{\sigma \Delta t}{2\varepsilon}$$

The discretization is made by cubic lattice on the simulation volume, and $\Delta x = \Delta y = \Delta$.

4. The data base requirement of the indoor wave propagation models

The geometrical description of the indoor scenarios are based on the same concept both for ray tracing and for FDTD methods The walls have to be partitioned to surrounding closed polygons and every such polygons are characterized by its electric material parameters.

The data base for the ray tracing method in our applications can not contain cut-out surfaces directly, such as windows, doors. Therefore the cut-out surface description is based on surface partitioning of the geometry as can be seen in *Figure 11*. The FDTD algorithm, on the contrary, allows application of simple ordinal database with overlapping polygons and the Yee cell parameter will be chosen by the simple decision that whichever object is higher on the list will overwrite the lower object in the mesh.

We prepared the indoor data base for a typical office building V2 at the Budapest University of Technology and Economics (BUTE), which has 7 floors and is made partially from concrete and brick. This data base for the sixth floor is used to make verification calculations and measurements of indoor wave propagation models and to develop new models. The floor plane is shown in *Figure 18*, and the floor view and polygonal partitioning in *Figure 13*, which is based on the previously described concept.

The data base contains the polygon coordinates, multiple and single layer wall types on the basis of *Table 3 (on the next page)*, for which the electrical material parameters of *Table 4* are used.

These parameters are partly results coming from literature, and from own material parameter measurements [14].

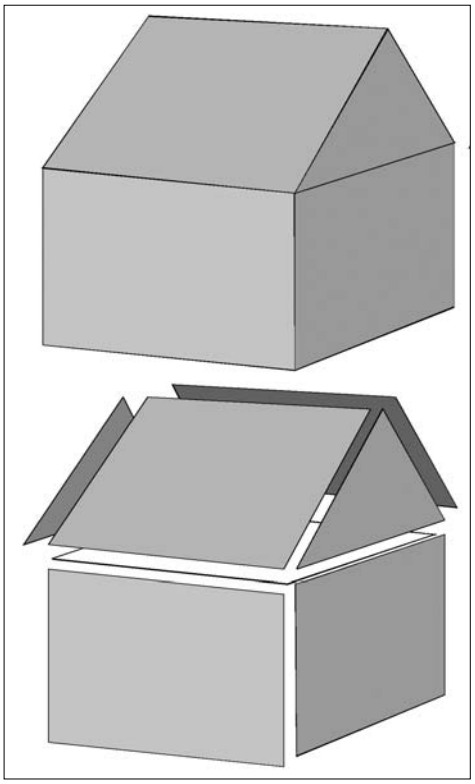

Figure 11. Polygon representation of building structure

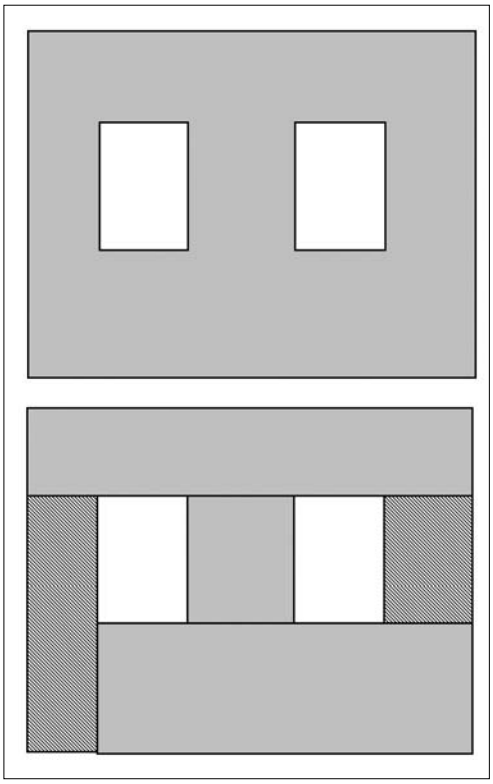

Figure 12. A possible polygonal partitioning of windowed walls for ray tracing method

Figure 13. Floor view and polygon data base of V2 building at BUTE

Type	Nr. of layers	Layer thicknesses
Brick	1	Brick – 6 cm
Brick	1	Brick – 10 cm
Brick	1	Brick – 12 cm
Brick + Concrete	3	Brick – 6 cm, Concrete – 20 cm, Brick – 6 cm
Brick + Concrete	3	Brick – 10 cm, Concrete – 12 cm, Brick – 10 cm
Brick + Concrete	3	Brick – 10 cm, Concrete – 10 cm, Brick – 10 cm
Brick	1	Brick – 15 cm
Concrete	1	Concrete – 15 cm
Concrete	1	Concrete – 20 cm
Concrete	3	Concrete – 15 cm, Air – 2 cm, Concrete – 15 cm
Glass	3	Glass – 3 mm, Air - 10 cm, Glass – 3 mm
Plasterboard	1	Plasterboard – 5 cm
Wood	1	Wood – 6 cm
Wood	1	Wood – 6 cm

Table 3.
Main wall types of indoor data base

These parameters of materials are specified either by the permittivity and loss tangent or directly by the complex permittivity, where $\varepsilon_r = \varepsilon'_r + j\cdot\varepsilon''_r = \varepsilon'_r - j\cdot(\tan\delta)\cdot\varepsilon'_r$.

Table 4. Electrical parameters of building materials

	Permittivity ε'_r	Loss tangent $\tan\delta$
Wood	3.5	0.01
Paper	3	0.008
Glass	5.5	0.001
Brick	2.8	0.2
Concrete	9	0.1

5. Application, results

Two ANSI C code were generated using the previous theory of general three-dimensional and of special two-dimensional FDTD methods for the two main cut of the cylindrical geometries. The methods are verified and results are presented for wave propagation problems.

5.1. Field strength distribution in the main two cut planes of tunnel

The application of the theory presented in Section 3 makes possible to investigate the mobile radio coverage in tunnels [13]. The axial plane field strength distribution in a tunnel with radius 2 m at the distance of 1 m from the axis of symmetry for sinusoidal excitation source by frequency of 900 MHz. The results are in good agreement with analytical results of literature [4].

The gradient of the linear regression to the FDTD simulation results in *Figure 14* is 9 dB/decade which indicates the waveguide nature of the tunnel at the frequency of investigation.

Figure 14.
Electrical field strength vs axial distance in tunnel

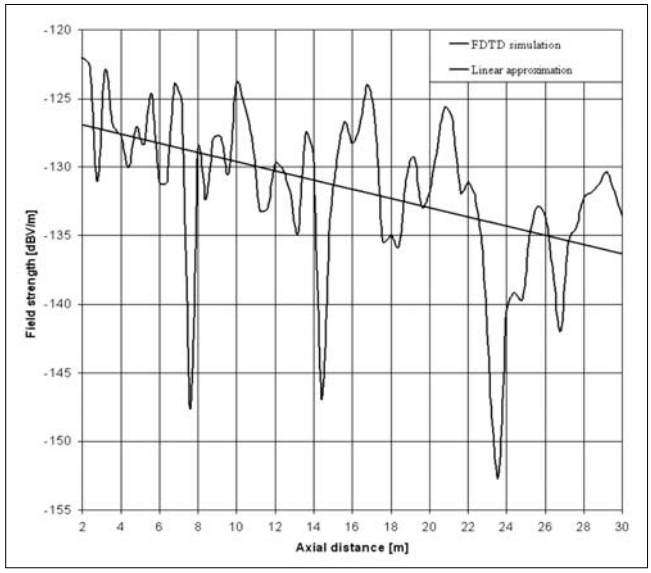

Figure 15. Field strength distribution of radial plane in tunnel without and with vehicle

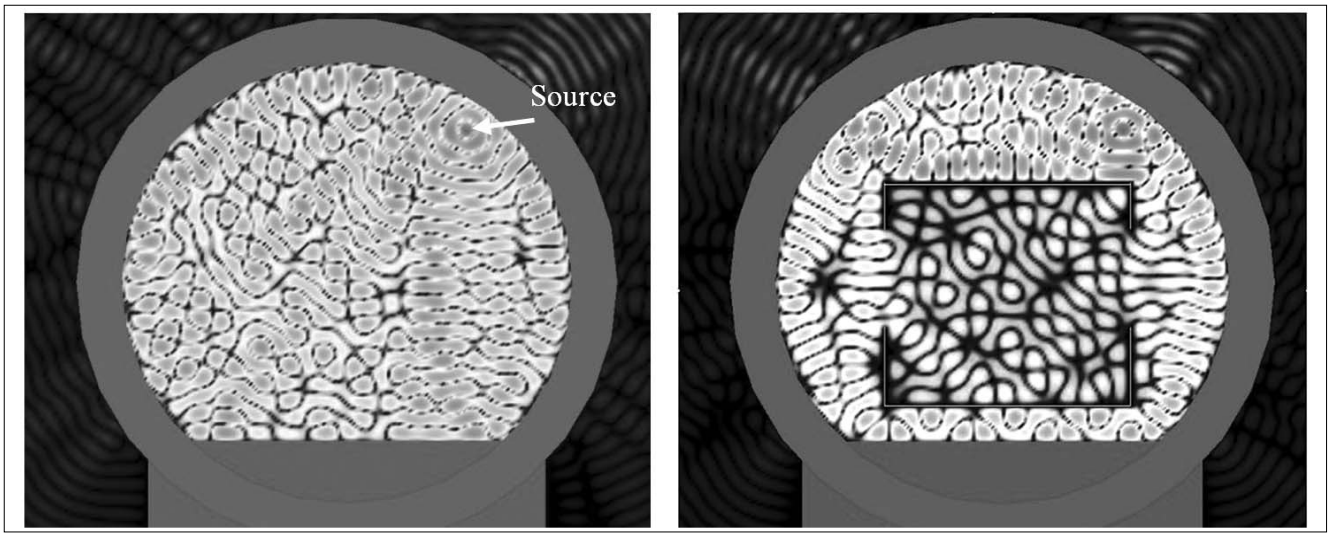

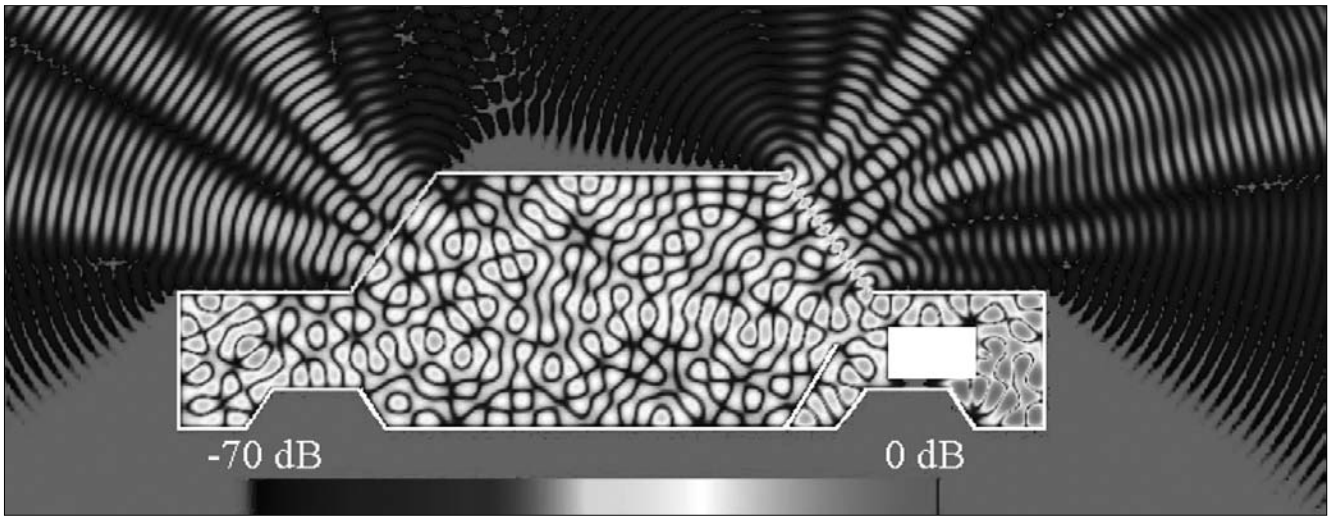

Figure 16. Stationary field strength distributions inside cars and radiated outside, caused by disturbing source from engine room at 1800 MHz

Our results in radial plane are shown as a two-dimensional electric field strength distribution in the tunnel and inside of the carriage for a point source with sinusoidal excitation.

The results illustrate very well how the field strength changes in presence of the underground carriage and how the propagating energy flows inside. The radial plane investigation gives a good opportunity for the optimization of the leaky cable for tunnel coverage and to determine the base station transmission power requirement for proper coverage inside of the vehicles.

Our next application areas are the EMC/EMI problems and additionally health risk analysis of electromagnetic waves. We demonstrate the stationary field strength distribution inside cars, caused by disturbing source from engine room *(Figure 16)*. Our next example is the induced electromagnetic field inside buildings generated by GSM base station *(Figure 17)*.

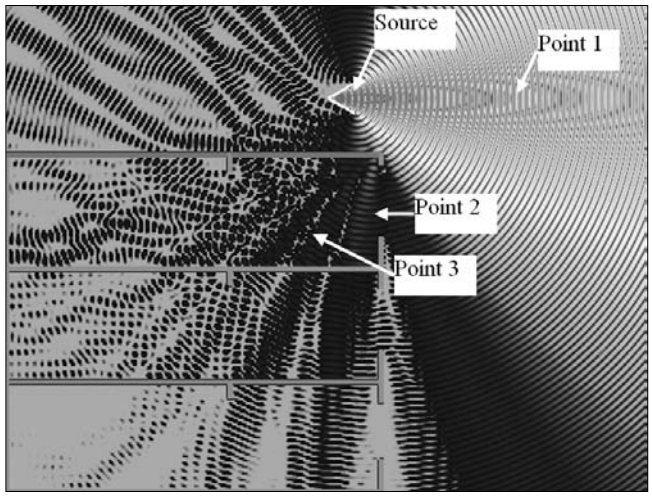

Figure 17. Stationary field strength distribution excited by a GSM base station at 900 MHz

The GSM base station coverage area at frequency of 900 MHz was investigated with FDTD using two-dimensional grid of 1 cm discretization and 1500x1700 grid size of area of simulation. The time step is specified as 19 ns and 3000 steps were calculated using PC with Centrino Duo processor working at 1.83 GHz. The simulation took 20 minutes and required 140 MB of operational RAM memory to store the field strengths. The walls are modeled as brick walls and as concrete ceiling, each having of 10 cm thickness.

In *Figure 17* in the interior space the field strengths at points 2 and 3 are less by a factor of 10^{-4} and 10^{-6} compared to the value at point 1. Using and improving the investigations outlined above the field levels of safety standards can be validated.

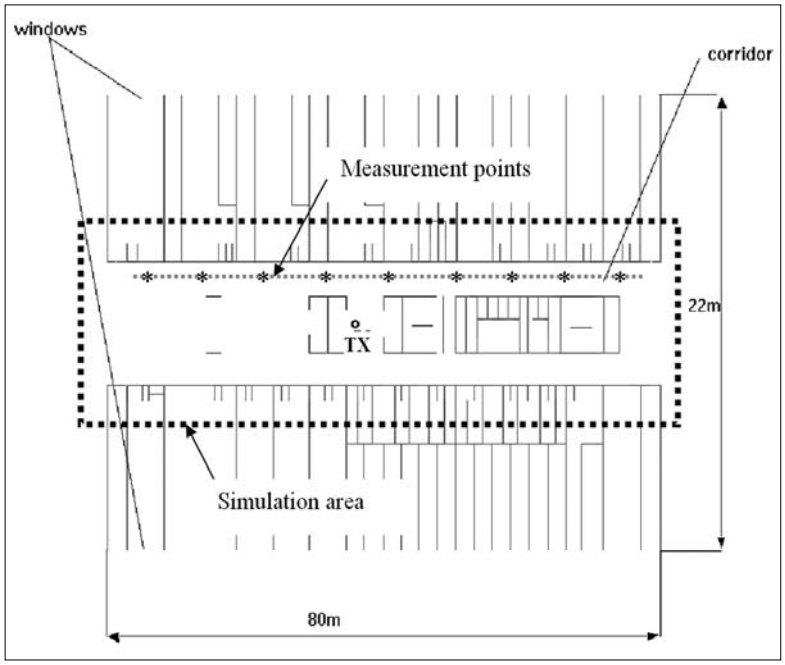

Figure 18. Indoor measurement scenario, floor plan with simulation area and measurement route

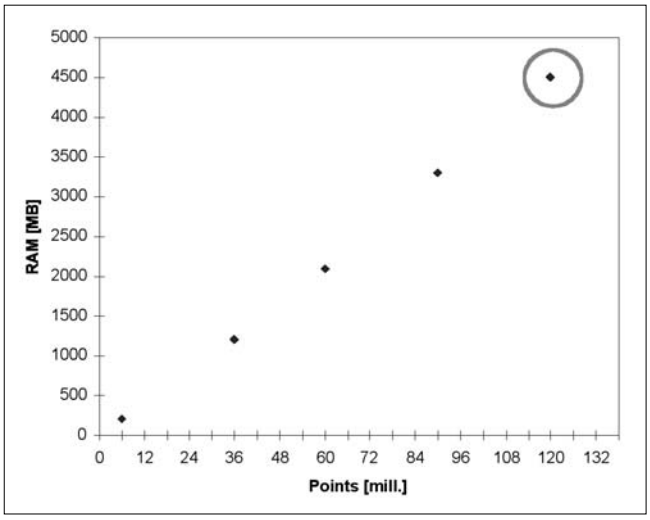

Figure 19.
Operational memory requirement of simulation

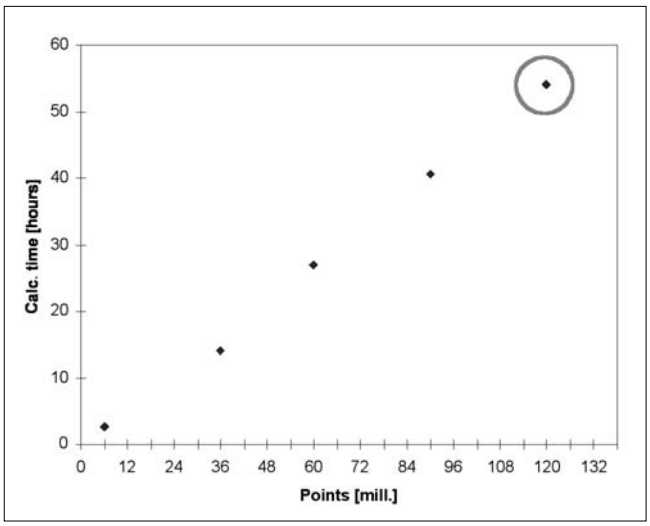

Figure 20. Running time requirement of simulation

Our last example will be the qualification of LPD short range radio links in indoor environment. The measurement and calculation results are shown at frequency of 433 MHz.

The building floor plan with measurement points on corridor and the area of simulation are presented in *Figure 18*. The simulation volume for FDTD has rectangular 90x11x3 cubic meter three dimensional size, and $\lambda/20 \approx 30$mm resolution of the FDTD results 120 million of Yee cells.

The running time and memory requirements of the simulation program is demonstrated in *Figures 19 and 20*, the values for present simulation are indicated.

Two quarter wavelength dipole was manufactured and vertically placed to perform the wireless channel measurements, spectrum analyzer was used for the received power and the channel attenuation measurements. At each spatial measurement points 500 received strength levels were measured and buffered for later processing. *Figure 21* compares measured minimum, maximum and average levels to simulated ones.

Excitation with sinusoidal time dependence is used to the FDTD simulation and at each spatial measurement points the recorded time function is transformed to frequency domain using Fourier transform. The received field level and radio link loss at frequency of 433 MHz was taken from this spectral distribution.

The comparative analyzis of simulations and measurements results in average difference of -1.74 dB and standard deviation of 15.5 dB. The average difference shows a fair agreement but the difficulty in channel modeling is indicated by the notable deviation and therefore the received field level estimation at individual spatial points only possible with high probability of error.

The most important parameter of the radio network design is the path loss exponent of the distance parameter, which is introduced for our investigation using the measurement results. The free space and two rays propagation models have path loss exponents of n=2 and n=4 respectively. On the contrary, our indoor short distance measurements have exponent of n=4.65 at frequency of 433 MHz, which was derived using linear regression to measurement path loss results presented in *Figure 22*.

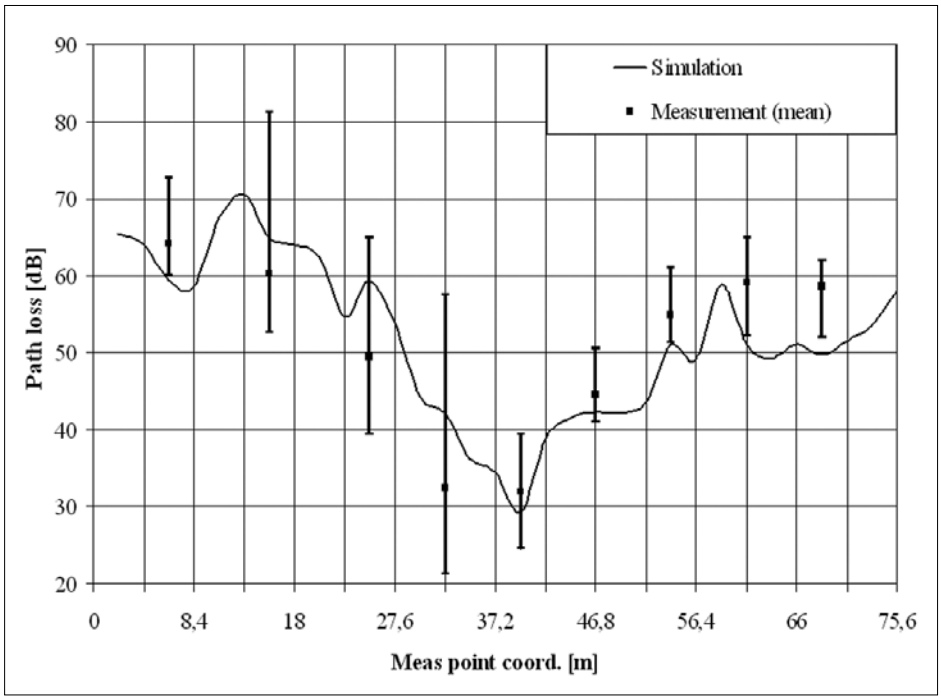

Figure 21.
Indoor path loss level comparison at frequency of 433 MHz (min, mean and max values for measurements are indicated)

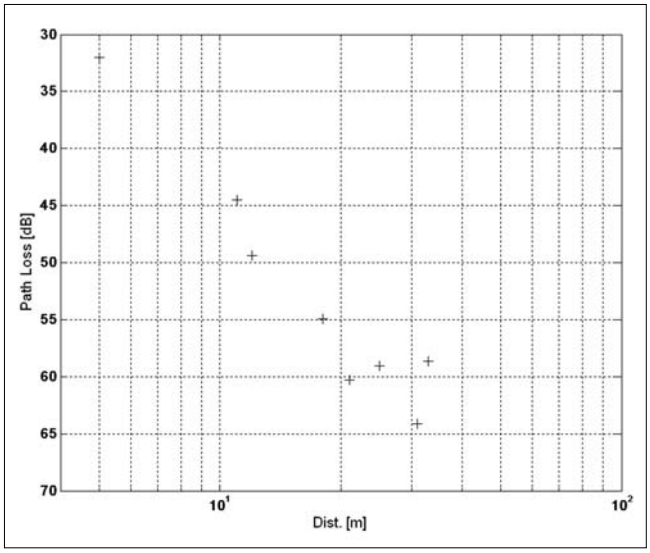

Figure 22.
Path loss dependence of measurement result at frequency of 433 MHz

6. Summary

Figures 19 and 20 present memory requirement of 4.5 GB and running time of 55 hours for the last 3 dimensional short range radio simulations. The resource requirement of simulation is increasing approximately by a factor of *frequency*^{3} for three-dimensional, and of *frequency*^{2} for two-dimensional geometry, and therefore the FDTD method can be applied only with significant limitations in simulation volumes, especially for simulations at higher frequencies .

The pure FDTD can improve by combining with ray tracing method. In this concept the ray tracing is performed to the border of a volume of detailed investigation and in this surrounding space of the receiver antenna FDTD method is applied using the ray traced field as excitation. Specific such problem is the characterization of MIMO (Multiple Input Multiple Output) radio channel, for which the combined method can be introduced. [12]

Acknowledgment

This work was carried out in the framework of Mobile Innovation Center, Hungary (Mobil Innovációs Központ).

References

[1] A. von Hippel,
Dielectric Materials and Applications,
Artech House, Boston, 1995.
[2] Lukas Müller, Walter Vollenweider,
Measurements of Radio Propagation in Buildings,
LPRA Conference, Birmingham, England,
October 29-31, 1996.
[3] Lambertus J.W. van Loon,
Mobile In-Home UHF Radio Propagation for
Short-Range Devices,
IEEE Antennas and Propagation Magazine,
Vol. 41., No.2, April 1999.
[4] Donald G. Dudley,
Wireless Propagation in Circular Tunnels,
IEEE Trans. Antennas Propagat.,
Vol. 53., pp.435–441., 2005.
[5] Allen Taflove, Susan C. Hagness,
Computational Electrodynamics:
The finite-difference time-domain method,
Artech House, Norwood, 2005.
[6] V. Rodrigez-Pereyra, A.Z. Elsherbeni, C.E. Smith,
A Body of Revolution Finite Difference
Time Domain Method with Perfectly Matched Layer
Absorbing Boundary, PIERS 24, pp.257–277., 1999.
[7] Yee, K.S.,
Numerical Solution of Initial Boundary Value Problems
Involving Maxwell's Equations in Isotropic Media,
IEEE Trans. Ant. Prop., Vol. 14., No.3, p.302., 1966.
[8] H. L. Bertoni,
UHF Predictions for Wireless Personal
Communications, Proceedings of the IEEE,
Vol. 82., No.9, pp.1333–1356., 1994.
[9] Constantine A. Balanis,
Advanced Engineering Electromagnetics,
John Wiley & Sons, 1989.
[10] Simon R. Saunders,
Antennas and Propagation for
Wireless Communication Systems, Wiley, 1999.
[11] Lajos Nagy,
FDTD Field Strength Prediction for Mobile Microcells,
ICECOM 2005 – 18th International Conference
on Applied Electromagnetics and Communications,
Dubrovnik, Croatioa, 12-14. October 2005.
[12] Lajos Nagy,
MIMO cube in realistic indoor environment,
EuCAP 2006 – The European Conference on
Antennas and Propagation,
Nice, France, 6-10. November 2006.
[13] Lajos Nagy,
Propagation modeling in subway tunnel using FDTD,
EuCAP 2006 – The European Conference on
Antennas and Propagation,
Nice, France, 6-10. November 2006.
[14] Lajos Nagy,
An Improved TDR Method for Determining Material
Parameters, XXIII. General Assembly of the URSI,
Prague, 1990.